Macroscopic gas ensembles as Quantum Memory

IISER PUNE

A thesis submitted towards partial fulfilment of
BS-MS Dual Degree Programme

by

M. Sainath

under the guidance of

Dr. Umakant D. Rapol

Assistant Professor

Department of Physics

Indian Institute of Science Education and Research Pune

Certificate

This is to certify that this thesis entitled **Macroscopic gas ensembles as Quantum Memory** submitted towards the partial fulfilment of the BS-MS dual degree programme at the Indian Institute of Science Education and Research Pune represents original research carried out by **M. Sainath** at **Indian Institute of Science Education and Research, Pune**, under the supervision of **Dr. Umakant D. Rapol** during the academic year 2014-2015.

Student

M. SAINATH

·25/3/2015

Supervisor

DR. UMAKANT D. RAPOL

Declaration

I hereby declare that the matter embodied in the report entitled **Macroscopic gas ensembles as Quantum Memory** are the results of the investigations carried out by me at the **Department of Physics, Indian Institute of Science Education and Research Pune**, under the supervision of **Dr. Umakant D. Rapol** and the same has not been submitted elsewhere for any other degree.

Student

M. SAINATH

25/3/2015

Supervisor

DR. UMAKANT D. RAPOL

Acknowledgements

Abstract

Manipulation and control of quantum systems has attracted a lot of attention in the recent decade due to enormous possibilities of simplifying the solution of certain physical and mathematical problems that were thought to be intractable with classical systems. Notable examples of such problems being the factorization of large numbers and solving the structure of complex molecules by utilizing the underlying complexity of quantum systems. Quantum information processing (QIP) deals with the use of the ability of manipulating and controlling the internal state of isolated quantum systems and the coupling of quantum systems for solving the above mentioned problems. In case of a QIP system, a single building block having two degrees of freedom is referred to as a Qubit (equivalent to bit in classical computers). There are variety of systems that have been studied extensively for usability in QIP. For e.g. Quantum optic systems (two level atoms and photons), solid state systems (Josephson junction), and NMR systems where an ensemble of molecules is used for QIP. The basic criteria for any system to qualify as a Qubit have been laid out by DiVincenzo. Most of the systems based on isolated single Qubits have been technically challenging to work with, for e.g. they require state of the art technologies in the area of Ultra high vacuum, lasers, optics and RF electronics. An alternative that has been proposed in the recent times has been to use macroscopic atomic vapour cells where the entire vapour cell acts as a single pure-Qubit. The collective internal electronic spin states of these atoms in the gaseous form is used a Qubit. The state of the Qubit is prepared through optical pumping and the spin state is read out through birefringence of the atomic vapor to the incident probe light. However, the challenging part in these systems is to increase the spin relaxation times. The spin relaxation normally is associated with the inelastic collisions between the atoms in the gas phase and walls of the cells. This thesis addresses the issue of increasing the spin relaxation time. It is well know that, spin relaxation time can be increased by coating the vapor cells with long hydrocarbon chains. The coatings like paraffin (Tetracontane) are known to allow a spin polarized atom to experience thousands of collisions with cell walls without getting depolarized. During the course of this Master's thesis, efforts have been made to fabricate paraffin coated glass vapor cells filled with Rubidium atoms and to characterize these cells.

Contents

Chapter 1

Introduction

Quantum systems possess features of superposition and entanglement exhibit exciting properties that open up possibilities for applications which were previously thought not possible using classical systems used as information processing devices. Amongst them popular applications like quantum computation would solve the problems which are believed to take exponentially longer time using the classical computers [1]. In addition cryptographic schemes designed with quantum mechanical systems would give more information security over the public channels [2]. The discovery of quantum algorithms for problems like Prime Factorization, Discrete Log problem by Peter Shor, Grover's search algorithm, and others by David Deutsch and Seth Lloyd which solve respective problems faster than their classical analogues. This has caught a lot of attention over the quantum information processing. These possibilities lead to the foundations of the field of quantum information. Even the programming language for a quantum computer like QCL, LanQ [3] have been created recently however the experimental realization of a Quantum Information Processor has still remained in its infancy.

For a system to qualify as a candidate for a quantum computer it requires to showcase the abilities to control and measure the quantum mechanical properties of the underlying system. The necessary conditions for such a system are given by D. Divincenzo[4] as follows

1. A scalable physical system with well characterized qubits.

2. The ability to initialize the state of the qubits to a simple pure state

3. Universal set of Quantum gates

4. Long decoherence times, much longer than the gate operation times.

5. Qubit-specific Measurement

Many physical systems like Nuclear Magnetic Resonance systems, solid state systems like Josephson junctions and Quantum optical systems satisfy most of the above criteria and are the amongst most studied systems in the context of quantum information. But the NMR based systems face the problem of scalability and solid state systems face the problems of short coherence times due to poor isolation of qubit environments. Due to these reasons physical systems from the field of atomic physics and quantum optics like Ions in electromagnetic traps and Cavity-QED systems with well understood environments and couplings tend to attract the current researchers. Although these systems also become more complex when scaled to higher number of qubits. These systems suffer

from extreme complexity involving state of the art techniques in Ultra-High Vacuum, RF electronics and stable laser systems. In order to reduce the complexity in realization of reliable Qubits there have been proposals to use atomic vapor cells as optical quantum memory elements. These systems are attractive because of their simplicity devoid of the other technical complexity. Here the macroscopic spin polarization of the atomic ensembles is used as a Qubit. However, technicalities involved in the construction of vapour cells that provide extremely large spin relaxation times still remain elusive.

1.1 Vapour cells as Quantum memory

A vapour cell or a warm atomic ensemble is a glass enclosure usually cylindrical in shape with macroscopic number of alkali atoms sealed under High Vacuum. These vapour cells are good for quantum memory applications since as mentioned earlier they do not require UHV, laser cooling which are needed for Ultracold atom, ion experiments and do not require cryogenics techniques as in the case of solid state systems. These properties give them the advantage over scalability and manufacturing. Thus they are widely used for many applications from spectroscopy, early laser cooling experiments and atomic clocks

1.1.1 History

Traditionally alkali vapour cells were being used for spectroscopy and magnetometry. For optimum performance many research groups invested a lot of efforts in improving the spin relaxation times in these cells. Through these initial efforts it was found that certain quantum mechanical properties could be efficiently measured and probed. This gave birth to the idea of using these cells for storage of quantum information. An idea that will be built on decades of research on atomic physics, quantum optics.

The first implementation of quantum memory using interaction between macroscopic atomic ensembles and optical fields was proposed by Duan, Lukin, Cirac, and Zoller(DLCZ) in 2000[5] which attracted considerable attention. The first experimental realizations of long-lived entanglement of two vapour cells was done by B. Julsgaard et al. [6] who used measurement and feedback to map polarization states of light onto the Cs vapour cells. Other experimental realizations demonstrated storage of light using electromagnetically-induced transparency (EIT) by two groups in 2001. The first group [7] used cold atomic ensemble and the other used ^{87}Rb vapour cell with He as buffer gas[8] who demonstrated the spin storage times of up to 200μs.
After these initial demonstrations many heated vapour cell experiments have been carried out and many other schemes were proposed by different groups[9]. These will be briefly summarized in next section.

1.1.2 Implementations of Optical Quantum memory

- **Optical Delay Lines and Cavities**: A loop of fiber is used to introduce delay which can be used as a quantum memory. Similarly, a simple optical cavity that has a high Q factor can be used to store light which bounces back and forth inside the cavity for a fixed time. These systems have advantages over bandwidths but have issues of power losses which limit their storage time. But when atoms are used in these cavities (Cavity-QED) systems due to their strong couplings give large storage times and can be used be as quantum memories.

- **Electromagnetically Induced Transparency**: EIT is a nonlinear optical phenomenon in three level atomic systems e.g. a three level Λ type system. When two optical fields couple two of the ground states to third common excited level then weak signal field will not be absorbed in presence of strong coupling field when the frequency difference is close to the frequency difference between the ground states, also called as the Raman detuning. In the absence of the control field, the weak probe field undergoes partial or complete absorption. If the intensity of coupling field is adiabatically reduced to zero, it follows that probe pulse gets trapped inside the atomic vapour which can be used as a memory. This idea of using EIT as quantum memory was first proposed by M. Fleishhauer et. al (2000) [10]

- **Off-Resonance Faraday Interactions**: A far detuned off-resonant light produces negligible absorption effects when compared to the dispersion effects. These dispersion effects can be used to read and write the polarization state of light in to a spin polarized atomic ensemble. This scheme of realization of quantum memory was first implemented by Julsgaard et.al [6]. More details about this scheme of Quantum Memory is discussed in Chapter2.

- **DLCZ Protocol**: Similar to EIT Quantum Memory, a scheme for creating long-lived entanglement was proposed by Duan, Lukin, Cirac and Zoller (DLCZ)[5]. First a collective excitation is created in a λ-type atoms which is created by the ensemble itself by the correlation between the emission of a Stokes photon and the collective excitation in an atomic ensemble which in turn is produced by a spontaneous Raman scattering.

Apart from the above mentioned implementations many other schemes like **Raman Memory**, **Photon Echo Memory** and **Gradient Echo Memory** are among the other popular implementations catching the interests of researchers.

1.1.3 Metrics of Quantum Memory

In last section we have seen some of the implementations of Quantum Memory but a candidate of quantum memory have specific requirements to be satisfied to be effective for Quantum information and computation.

- **Efficiency**: It is the ratio of intensity of the output light which is read out to the intensity of the input light which was used to write the state. This gives how efficient the memory can be in terms of energy losses. For systems with low efficiency rates there is a necessary to use Quantum error correcting protocols in the applications like quantum computing.

- **Fidelity**: It refers to the overlap of initial wave function to the final wave function read out from the memory. It should be sufficiently large than the worst case fidelity of the system below which the error correction algorithms fail to be effective.

- **Storage time**: The memory needs to be able to store the information long enough so that we can perform the specific quantum information task. Thus this is an important performance criteria.

In addition to the above, other criteria like having more bandwidth, ability to have multi-mode capacity are also required for a good quantum memory.

1.2   Overview and Outline

As we have seen in previous sections, realizations of quantum memory for light using vapour cells is promising and rapidly developing field and results show efficient storage, lifetime, fidelity and long lifetime. However these performance characteristics have been demonstrated using different protocols and more efforts are required for combining these benchmarks into one single protocol. To add to current research we would like to understand and improve the schemes for this type of realization of Quantum information, to enhance the benchmarks of these quantum memories. Due to the availability of established state of art laser system used for the ^{87}Rb Bose Einstein Condensate experiments, we are motivated to establish a multipurpose experimental setup using Rubidium vapour cells which can be used to demonstrate fundamental quantum information protocols like entanglement, teleportation etc., In this thesis we will be discussing the preparation and characterization of these natural mixture rubidium vapour cells which exhibit higher lifetimes. Special protocols have to be followed to prepare these cells in-house to show less decoherence effects. In chapter 2 we will be discussing basic formalism of atoms and light which we are interested in the context of the manipulation of the spin states of atoms in these vapour cells. We will be briefly presenting the formalism of off-resonant faraday interaction scheme. Then we will understand more about the life time of the spin states of vapour cells, important relaxation mechanisms. In chapter 3 the details of in-house fabrication of paraffin(tetracontane) coated vapour cells is described followed by a detailed description of a experimental setup required for measuring the spin relaxation lifetime of the cell. Later in Chapter 4&5 preliminary results are presented with short discussion, conclusion and future plans.

Chapter 2

Atom Light Interactions

In this chapter we are going to discuss some basic quantum mechanical properties of light and atoms which are relevant in our experiments. We need to be able to device a formalism to exchange the degrees of freedom between atoms and light to be able to store the quantum information. Then we will be discussing the actual physical picture we are going to consider during the course of the experiment. Later we will be discussing in the context of vapour cells the mechanisms of relaxation.

2.1 Light

Electric field in a free space satisfies the wave equation given be

$$\nabla^2 \mathbf{E}(r,t) = \frac{1}{c^2} \frac{\partial^2 \mathbf{E}(r,t)}{\partial t^2}$$

Consider an electromagnetic radiation in a confined hypothetical cavity. In this cavity EM field can only excite to discrete spatial modes, which have to satisfy the boundary conditions that electric field $\mathbf{E}$ must vanish at the boundaries. The solution with such constraints is given by

$$E_x(r,t) = E_x(t)\cos(k_x x)\sin(k_y y)\sin(k_z z)$$

where $k_i = \frac{\pi v_i}{L}$ for $i = x, y, z$ and L is the length of the cavity.
From the above boundary conditions and the fact that $\nabla.\mathbf{E} = 0$, we get the condition that $\mathbf{k}.\mathbf{E}(t) = 0$ which in turn implies that E is perpendicular to k vector. Thus for each wave vector 2 possible directions exist which we are going to denote as $\lambda = 1, 2$. This gives rise to two basic states of polarization. In the following sections we will see how this polarization can be formulated in quantum mechanics.

2.1.1 Quantization of Electromagnetic Field

Till now we have considered the classical formalism of EM field, in this section we will try to quantize the electromagnetic field. Initial part of this section is adapted from Ref. [11] and is presented in brief.
    To get the quantum mechanical equivalent of the electric and magnetic fields we

consider the vector potential $\mathbf{A}$ and scalar potential ϕ defined by

$$\mathbf{B} = \nabla \times \mathbf{A}$$

$$\mathbf{E} = -\nabla\phi - \frac{\partial \mathbf{A}}{\partial zt}$$

Substituting the above into the Maxwell's equations $\nabla.\mathbf{E} = \frac{\rho}{\epsilon_0}$ and $\nabla \times \mathbf{b} = \mu_0(\mathbf{J} + \epsilon_0 \frac{\partial \mathbf{E}}{\partial t})$ we get the field equations

$$\nabla(\nabla.\mathbf{A}) - \nabla^2\mathbf{A} + \frac{1}{c^2}\frac{\partial}{\partial t}\nabla\phi + \frac{1}{c^2}\frac{\partial^2\mathbf{A}}{\partial t^2} = \mu_0 J$$

$$-\epsilon_0\nabla^2\phi - \epsilon_0\nabla.\left(\frac{\partial \mathbf{A}}{\partial t}\right) = \sigma$$

Applying the Coulomb gauge $\nabla.\mathbf{A} = 0$ the field equations transform into

$$-\nabla^2\mathbf{A} + \frac{1}{c^2}\frac{\partial}{\partial t}\nabla\phi + \frac{1}{c^2}\frac{\partial^2\mathbf{A}}{\partial t^2} = \mu_0\mathbf{J} \qquad (2.1)$$

$$-\nabla^2\phi = \frac{\sigma}{\epsilon_0}$$

The Helmholtz's decomposition theorem from vector calculus states that any vector field can be decomposed into a curl-free component and divergence-free component. Thus we divide the current density $\mathbf{J}$ into two components $\mathbf{J_T}$ which is divergence free component and $\mathbf{J_L}$ which is curl free component. Using this eqn. 2.1 is decomposed into two equations

$$-\nabla^2\mathbf{A} + \frac{1}{c^2}\frac{\partial^2\mathbf{A}}{\partial t^2} = \mu_0\mathbf{J_T} \qquad (2.2)$$

$$\frac{1}{c^2}\frac{\partial}{\partial t}\nabla\phi = \mu_0\mathbf{J_L}$$

In free space we consider the transverse component of $\mathbf{J_T} = \mathbf{0}$. Thus we get the wave equation of vector potential from the eqn. 2.2

$$-\nabla^2\mathbf{A} + \frac{1}{c^2}\frac{\partial^2\mathbf{A}}{\partial t^2} = 0$$

Now consider a hypothetical cavity of length L and periodic boundary conditions. The solution for the vector potential would be given as

$$\mathbf{A}(r,t) = \sum_k \sum_{\lambda=1,2} \mathbf{e}e_{\mathbf{k}\lambda}A_{\mathbf{k}\lambda}(\mathbf{r},t)$$

where $\mathbf{e}_{\mathbf{k}\lambda}$ are the unit polarization vectors and $A_{\mathbf{k}\lambda}$ is given by

$$A_{\mathbf{k}\lambda}(r,t) = A_{\mathbf{k}\lambda}(t)e^{i\mathbf{k}.\mathbf{Ar}} + A_{\mathbf{k}\lambda}^*(t)e^{-i\mathbf{k}.\mathbf{r}} \qquad (2.3)$$

as we are working in Coulomb gauge $\nabla.\mathbf{A} = 0$ this implies that $\mathbf{e}_{\mathbf{k}\lambda}.\mathbf{k} = 0$. We choose polarization vectors to be perpendicular to each other $\mathbf{e}_{\mathbf{k}\lambda}.\mathbf{e}_{\mathbf{k}\lambda'} = \delta_{\lambda\lambda'}$. Applying this condition we can see that each $A_{\mathbf{k}\lambda}$ satisfies

$$\frac{\partial^2 A_{\mathbf{k}\lambda}(t)}{\partial t^2} + c^2k^2 A_{\mathbf{k}\lambda}(t) = 0$$

which is an equation of a harmonic oscillator whose solution can be given as

$$A_{\mathbf{k}\lambda}(t) = A_{\mathbf{k}\lambda}e^{-i\omega_k t}$$

Substituting the above into eq.2.3 we get

$$A_{\mathbf{k}\lambda}(r,t) = A_{\mathbf{k}\lambda}e^{(-ickt+i\mathbf{k}.\mathbf{r})} + A_{\mathbf{k}\lambda}^*e^{(ickt-i\mathbf{k}.\mathbf{r})}$$

From the above equation expressions for $\mathbf{E}$ and $\mathbf{B}$ can be calculated as follows

$$
\begin{aligned}
\mathbf{E}_T(r,t) &= \sum_{\mathbf{k}}\sum_{\lambda=1,2} \mathbf{e}_{\mathbf{k}\lambda}\left(-\frac{\partial A_{\mathbf{k}\lambda}(r,t)}{\partial t}\right) \\
&= \sum_{\mathbf{k}}\sum_{\lambda=1,2} \mathbf{e}_{\mathbf{k}\lambda}\left(i\omega_k(A_{\mathbf{k}\lambda}e^{(-i\omega_k t+i\mathbf{k}.\mathbf{r})} - A_{\mathbf{k}\lambda}^*e^{(i\omega_k t-i\mathbf{k}.\mathbf{r})})\right)
\end{aligned}
\tag{2.4}
$$

$$
\begin{aligned}
\mathbf{B}(r,t) &= \sum_{\mathbf{k}}\sum_{\lambda=1,2} \nabla \times (\mathbf{e}_{\mathbf{k}\lambda}A_{\mathbf{k}\lambda}(r,t)) \\
&= \sum_{\mathbf{k}}\sum_{\lambda=1,2} \frac{\mathbf{k}\times e_{\mathbf{k}\lambda}}{k}\left(ik(A_{\mathbf{k}\lambda}e^{(-i\omega_k t+i\mathbf{k}.\mathbf{r})} - A_{\mathbf{k}\lambda}^*e^{(i\omega_k t-i\mathbf{k}.\mathbf{r})})\right)
\end{aligned}
\tag{2.5}
$$

Now we try to calculate the total energy of Electromagnetic field inside a cavity given as

$$E_R = \frac{1}{2}\int_{cavity} dV \left(\epsilon_0\mathbf{E}_T^2 + \frac{1}{\mu_0}\mathbf{B}^2\right)$$

substituting the expressions for $\mathbf{E}_T$ and $\mathbf{B}$ from 2.4 and 2.5

$$E_R = \sum_{\mathbf{k}}\sum_{\lambda} \epsilon_0 V\omega_k^2(A_{\mathbf{k}\lambda}A_{\mathbf{k}\lambda}^* + A_{\mathbf{k}\lambda}^*A_{\mathbf{k}\lambda}) \tag{2.6}$$

This equation is similar to the hamiltonian of a harmonic oscillator with the creation operator $\hat{a}^\dagger$ and annihilation operator $\hat{a}$ which can be expressed as

$$\hat{H} = \frac{1}{2}\hbar\omega(\hat{a}\hat{a}^\dagger + \hat{a}^\dagger\hat{a})$$

Comparing the above equation with eqn. 2.6 we can see that to get a quantum mechanical hamiltonian for Electromagnetic radiation we can just assign a harmonic oscillator for each mode $\mathbf{k}\lambda$. Thus the hamiltonian for electromagnetic radiation is given as

$$H_R = \sum_{\mathbf{k}}\sum_{\lambda} \hat{H}_{\mathbf{k}\lambda}$$

$$\hat{H}_{\mathbf{k}\lambda} = \frac{1}{2}\hbar\omega_k(\hat{a}_{\mathbf{k}\lambda}\hat{a}_{\mathbf{k}\lambda}^\dagger + \hat{a}_{\mathbf{k}\lambda}^\dagger\hat{a}_{\mathbf{k}\lambda})$$

Here each creation operator $\hat{a}_{k\lambda}$ creates and annihilation operator $\hat{a}_{k\lambda}^\dagger$ destroys a photon of energy $\hbar\omega_k$ in mode $k\lambda$. The eigen states of the hamiltonian $|n_{k\lambda}\rangle$ are called the **Fock states** of Electromagnetic field. The Eigen value equation for these states is given as

$$\hat{H}_R|n_{\mathbf{k}\lambda}\rangle = \sum_{\mathbf{k}}\sum_{\lambda} \hbar\omega_k(n_{\mathbf{k}\lambda} + \frac{1}{2})|n_{\mathbf{k}\lambda}\rangle$$

In terms of creation operators $\hat{a}_{k\lambda}^{\dagger}$ a fock state is given by

$$|n_{k\lambda}\rangle = \frac{1}{\sqrt{n!}}(\hat{a}^{\dagger})^n |0\rangle \qquad (2.7)$$

Now from the comparison of Hamitonian and energy expression we get motivated to replace the vector potential $A_{k\lambda}$ in terms of $\hat{a}_{k\lambda}$ and $\hat{a}_{k\lambda}^{\dagger}$ as follows

$$A_{\mathbf{k}\lambda} \rightarrow \left(\frac{\hbar}{2\epsilon_0 V \omega_k}\right)^{\frac{1}{2}} \hat{a}_{\mathbf{k}\lambda}$$

$$A_{\mathbf{k}\lambda}^{*} \rightarrow \left(\frac{\hbar}{2\epsilon_0 V \omega_k}\right)^{\frac{1}{2}} \hat{a}_{\mathbf{k}\lambda}^{\dagger}$$

From the above, the expression for the electric field can be written in terms of creation and annihilation operators by using eqn. 2.4

$$\hat{\mathbf{E}}_{\mathbf{T}} = \sum_{\mathbf{k}} \sum_{\lambda} \left(\frac{\hbar\omega_k}{2V\epsilon_0}\right)^{\frac{1}{2}} \left[\hat{a}_{\mathbf{k}\lambda}\mathbf{e}_{\mathbf{k}\lambda}e^{-i(\omega_k t - \mathbf{k}.\mathbf{r} - \pi/2)} + \hat{a}_{\mathbf{k}\lambda}^{\dagger}\mathbf{e}_{\mathbf{k}\lambda}^{*}e^{i(\omega_k t - \mathbf{k}.\mathbf{r} - \pi/2)}\right]$$

In the context of our experiment let us consider that the light is propagating in positive-z direction and the extent of interaction is much larger that the wavelength itself. After making the overall phase change we get

$$\hat{\mathbf{E}} = \sum_{\mathbf{k}} \sum_{\lambda} \left(\frac{\hbar\omega_k}{2V\epsilon_0}\right)^{\frac{1}{2}} \left[\hat{a}_{\mathbf{k}\lambda}\mathbf{e}_{\mathbf{k}\lambda}e^{-i(\omega_k t - kz)} + \hat{a}_{\mathbf{k}\lambda}^{\dagger}\mathbf{e}_{\mathbf{k}\lambda}^{*}e^{i(\omega_k t - kz)}\right] \qquad (2.8)$$

2.1.2 Stokes Operators

Classically Stokes parameters are the values that describe the polarization states of the electromagnetic radiation. In terms of components of electric field they are defined as

$$S_0 = I \quad = \quad < E_x^2 > + < E_y^2 > \qquad (2.9)$$
$$S_1 = Q \quad = \quad < E_x^2 > - < E_y^2 > \qquad (2.10)$$
$$S_2 = U \quad = \quad < E_{+45}^2 > - < E_{-45}^2 > \qquad (2.11)$$
$$S_3 = V \quad = \quad < E_{\sigma+}^2 > + < E_{\sigma-}^2 > \qquad (2.12)$$

Now from the eqn. 2.8 we take single longitudinal mode with wave vector to be $\mathbf{k}$ and removing the time dependence by considering $\mathbf{E}$ at $t = 0$

$$\hat{\mathbf{E}}_k = \sum_{\lambda} \left(\frac{\hbar\omega_k}{2V\epsilon_0}\right)^{\frac{1}{2}} \left[\hat{a}_{\mathbf{k}\lambda}\mathbf{e}_{\mathbf{k}\lambda}e^{ikz} + \hat{a}_{\mathbf{k}\lambda}^{\dagger}\mathbf{e}_{\mathbf{k}\lambda}^{*}e^{-ikz}\right]$$

If we decompose electric field into x and y components with unit vectors $\mathbf{e}_x$, $\mathbf{e}_y$ and respective creation and annihilation operators

$$\hat{\mathbf{E}}_k = \left(\frac{\hbar\omega_k}{2V\epsilon_0}\right)^{\frac{1}{2}} \left[(\hat{a}_x\mathbf{e}_x + \hat{a}_y\mathbf{e}_y)e^{ikz} + (\hat{a}_x^{\dagger}\mathbf{e}_x^{*} + \hat{a}_y^{\dagger}\mathbf{e}_y^{*})e^{-ikz}\right] \qquad (2.13)$$

We define new unit vectors $\mathbf{e}_{\pm 1}$ and new creation, annihilation operators as

$$\mathbf{e}_{\pm 1} = \mp \frac{\mathbf{e}_x \pm i\mathbf{e}_y}{\sqrt{2}} \text{ and } \hat{a}_{\pm} = \mp \frac{\hat{a_x} \mp i\hat{a_y}}{\sqrt{2}} \tag{2.14}$$

To get $\hat{E}_k$ in terms of eqn. 2.15 we get

$$\hat{\mathbf{E}}_k = \left(\frac{\hbar \omega_k}{2V\epsilon_0} \right)^{\frac{1}{2}} \left[(\hat{a}_+ \mathbf{e}_{+1} + \hat{a}_- \mathbf{e}_{-1}) e^{ikz} + (\hat{a}_+^\dagger \mathbf{e}_{+1}^* + \hat{a}_-^\dagger \mathbf{e}_{-1}^*) e^{-ikz} \right] \tag{2.15}$$

From equations 2.13 and 2.15 we define stokes operators (2.9 to 2.12) interms of the creation and annihilation operators as

$$\hat{S}_x = \frac{1}{2}(\hat{a}_x^\dagger \hat{a}_x - \hat{a}_y^\dagger \hat{a}_y) \tag{2.16}$$

$$\hat{S}_y = \frac{1}{2}(\hat{a}_x^\dagger \hat{a}_y + \hat{a}_y^\dagger \hat{a}_x) \tag{2.17}$$

$$\hat{S}_z = \frac{1}{2}(\hat{a}_x^\dagger \hat{a}_y - \hat{a}_y^\dagger \hat{a}_x) \tag{2.18}$$

To understand the above operators it can be thought that expectations of $\hat{S}_x$ gives the number of x(horizontal) polarized photons minus y(vertical) polarized photons, $\hat{S}_y$ gives the photon count difference for polarizations along $\mathbf{e}_{+45}$ and $\mathbf{e}_{-45}$ and similarly $\hat{S}_z$ for σ_+ and σ_- photons. It can also be easily verified that the above mentioned stokes operators satisfy the commutation relations given by

$$\left[\hat{S}_a, \hat{S}_b \right] = i\epsilon_{abc}\hat{S}_c \tag{2.19}$$

where a, b, c are indices and ϵ_{abc} is the Levi-Civita symbol.

Now we have constructed a formalism for polarization of electromagnetic radiation in terms stokes operators, we then aim to build a similar formalism for ensemble of atoms to couple their degree of freedom.

2.2 Atoms

2.2.1 Spin Quantization for Ensemble of atoms

Since we are working with ensemble of atoms and there is no way to probe each atom, only some properties of entire ensemble of atoms can be measured. So, our formalism should have operators which act on entire state of atoms. In the context of our experiment what we are interested in, is the collective angular momentum of collection of atoms.

For an atom the angular momentum operator $\mathbf{J}$ defined by $\mathbf{J} = \mathbf{q} \times \mathbf{p}$ has components defined by $\hat{j}_x, \hat{j}_y, \hat{j}_z$. These components follow the commutation relations given as

$$\left[\hat{j}_a, \hat{j}_b \right] = i\hbar\epsilon_{abc}\hat{j}_c \tag{2.20}$$

where a, b, c are component indices and ϵ_{abc} is Levi-Civita symbol.

The angular momentum eigen states of $\hat{j}^2$ and $\hat{j}_z$ are denoted as $|j, m\rangle$

$$\hat{j}^2 |j, m\rangle = \hbar^2 j(j+1) |j, m\rangle$$
$$\hat{j}_z |j, m\rangle = \hbar m |j, m\rangle$$

The operators $\hat{j}_{\pm}$(raising and lowering operators) are defined as $\hat{j}_{\pm} = \hat{j}_x \pm i\hat{j}_y$. When these act on the eigen states they raise or lower the eigen state

$$\hat{j}_{\pm} |j, m\rangle = \hbar\sqrt{j(j+1) - m(m \pm 1)} |j, m \pm 1\rangle$$

Now if we consider an ensemble of identical atoms we can represent the internal state of N atoms in a corresponding Hilbert space of 2^N dimensions by introducing a collective spin operator as

$$\hat{J} = \sum_{i=1}^{N} \hat{j}^{(i)} \tag{2.21}$$

where $j^{(i)}$ is total angular momentum of ith atom. In this case the simultaneous eigen state of $\hat{J}^2$ and $\hat{J}_z$ is called a **Dicke State** and the eigen value equation is given as

$$\hat{J}^2 |J, M\rangle = \hbar J(J+1) |J, M\rangle$$
$$\hat{J}_z |J, M\rangle = \hbar M |J, M\rangle$$

where the value of M ranges from $-J$ to J. Similarly the raising and lowering operators can be defined as

$$\hat{J}_{\pm} |J, M\rangle = \hbar\sqrt{J(J+1) - M(M \pm 1)} |J, M \pm 1\rangle$$

It follows that when a raising operator acts on the ground state $|J, -J\rangle$ repeatedly we get

$$\hat{J}_+ |J, -J\rangle = \sqrt{2J} |J, -J+1\rangle \tag{2.22}$$
$$\hat{J}_+ |J, -J+1\rangle = \sqrt{2(2J-1)} |J, -J+2\rangle \tag{2.23}$$
$$\cdot$$
$$\cdot$$
$$\cdot$$
$$\hat{J}_+ |J, M-1\rangle = \sqrt{(J+M)(J-M+1)} |J, M\rangle \tag{2.24}$$
$$\tag{2.25}$$

combining equations from 2.22 to 2.24 we get

$$|J, M\rangle = \frac{1}{(J+M)!} \left(\begin{array}{c} 2J \\ J+M \end{array}\right)^{1/2} \hat{J}_+^{(M+J)} |J, -J\rangle \tag{2.26}$$

We can see that above eqn. 2.26 is analogous to the photon number state (fock state) given by eqn. 2.7.

The collective angular momentum operators $\hat{J}_x$, $\hat{J}_y$, $\hat{J}_z$ also satisfy the commutation relations similar to that of eqn. 2.20

$$\left[\hat{J}_a, \hat{J}_b\right] = i\hbar\epsilon_{abc}\hat{J}_c \tag{2.27}$$

again, we can see that the above equation is analogous to 2.19. Thus by these comparisons we can see that we have built a similar formalism for both light and the collection of atoms. Now we will consider a specific case of ensemble of Rubidium atoms which we are interested in the course of the thesis work.

2.2.2 Ensemble of Rb atoms

In this thesis, we are going to work with an ensemble of Rubidium atoms of natural abundance. The reason is mainly due to availability of desired lasers at the wavelength of D_2 transition of Rb. Rubidium is alkali metal with atomic number 37 and atomic mass 85.46. The natural mixture of Rb mainly constitutes 2 isotopes - ^{85}Rb with abundance 72.2% and ^{87}Rb with an abundance of 27.8%. The energy level diagram of Rubidium is shown in the following Fig. 2.1, showing its $5S_{1/2} \rightarrow 5P_{1/2}$ (D1) transition and $5S_{1/2} \rightarrow 5P_{3/2}$ (D2) transition.
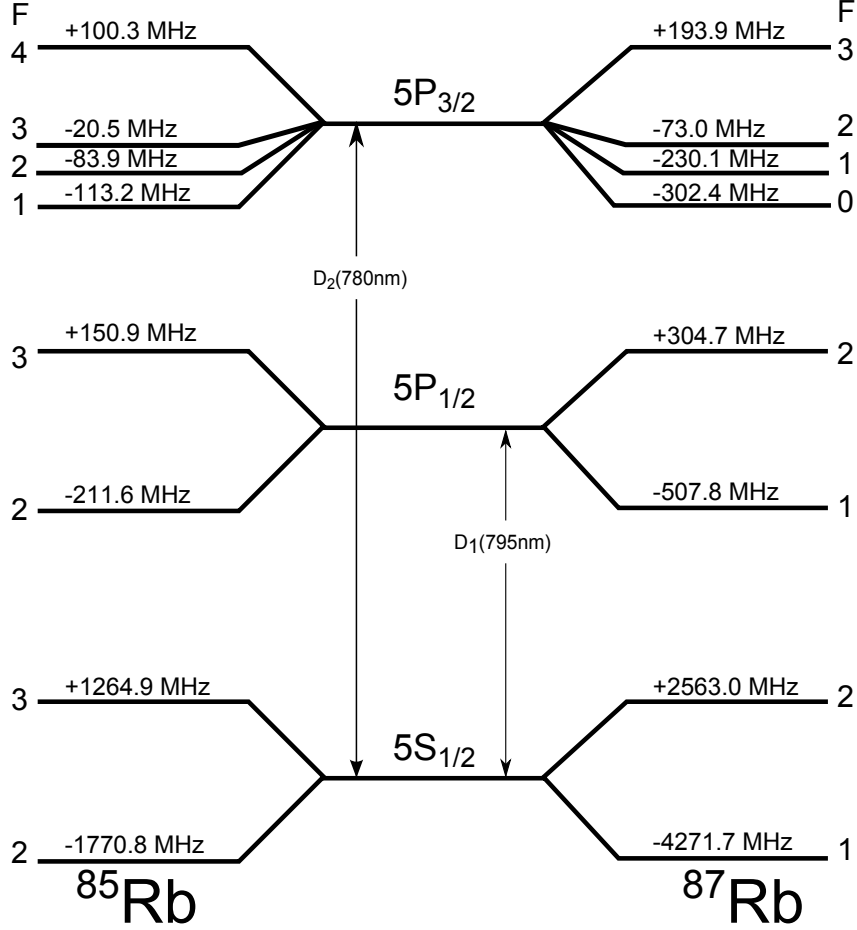

Figure 2.1: Energy Levels of ^{85}Rb and ^{87}Rb, Hyperfine Intervals taken from Ref. [12],[13]

It has ground state electronic configuration $[Kr]5s^1$ with one electron in the valence shell thus its orbital angular momentum L is zero and the total electronic angular momentum $J = L + S$ is given as $J = S = 1/2$. The coupling between the angular momentum J and the nuclear spin I gives rise to the hyperfine coupling with $F = I + J$. The nuclear spin of ^{87}Rb and ^{85}Rb are 3/2 and 5/2 respectively and the total angular momentum $F = I + J$ has the quantum numbers $F = 1$, $F = 2$ for ^{87}Rb and $F = 2$, $F = 3$ for ^{85}Rb.

As discussed in sec. 2.2.1 we are interested in total angular momentum. In the following experiments we aim to polarize almost all atoms along the direction of quantization axis (say z-axis). If we were able to transfer all the atoms into $F = 2, m_F = 2$ Zeeman sublevel. In case of ^{87}Rb or $F = 3, m_F = 3$ Zeeman level in case of ^{85}Rb we will be

aligning the atoms along the quantization axis. This is done through optical pumping (described in sec. 2.4). For this special case the expectation value of the operator $\hat{J}_z$ is high compared to that of $\hat{J}_x$ and $\hat{J}_y$ and thus can be treated as a classical variable say J_z while the other two components maintain their quantum nature. The commutation relation from eqn. 2.27 can then be written as

$$\left[\hat{J}_x, \hat{J}_y\right] = i\hbar\hat{J}_z$$

This sets the bound for uncertainty for the transverse components $\hat{J}_z$ and $\hat{J}_y$ from Heisenberg relation as

$$\Delta\hat{J}_x . \Delta\hat{J}_y \geq \frac{\hbar}{2}J_z$$

Similarly if we consider incident light to be horizontally polarized then number of photons with horizontal polarization is very large when compared to number of photons with vertical polarization. This follows that the expectation of stokes vector $\hat{S}_x$ from eqn. 2.16 is large and can be considered as a classical variable say S_x. Thus the commutation relation 2.19 transforms to

$$\left[\hat{S}_y, \hat{S}_z\right] = iS_x$$

Again this fixes the limit on the extent of uncertainty of $\hat{S}_z$ and $\hat{S}_y$.

$$\Delta\hat{S}_y . \Delta\hat{S}_z \geq \frac{1}{2}S_x$$

Now that we have understood the stokes parameters and collective spin in case of our vapour cell, we will briefly be describing the off resonant Faraday Interaction scheme implementing which was the main motivation of this thesis. This scheme is clearly described by B. Julsgaard in [14] but a simple description is given in the next section.

2.3   Off Resonant Faraday Interaction

Consider an ensemble of atoms polarized towards the quantization axis provided by a magnetic bias field. If we pass laser light with a detuning Δ from the transition frequency into the ensemble the interaction can be of two types, absorption and dispersion. In our case say the laser is locked to say $(5S_{1/2}, F = 2) \rightarrow (5P_{1/2}, F' = 3)$ transition with the detuning Δ. For a given intensity of light the absorption effects of the ensemble is proportional to $\frac{1}{\Delta^2}$ and dispersion effects are proportional to $\frac{1}{\Delta}$. So, for a large enough detuning the dispersion effect dominates over the absorption effects. For such large detuning the absorption by atoms is negligible and the entire ensemble can be thought of interacting with the polarization of light like a birefringent material.

To understand the birefringence let us consider a situation where atoms are aligned towards the z-axis and incident light propagating along z-axis is linearly polarized towards x-axis as shown in Fig. 2.2 Since the atomic ensemble has a preferred direction along the z-axis and has symmetry along other directions. Clearly we can see that the refractive index $n_{\sigma+} \neq n_{\sigma-}$, where as $n_x = n_y$. Thus the ensemble can be said to have a circular birefrengence which will lead to relative rotation of the polarization. Since the linearly polarized light can be thought as superposition of the circularly polarized lights, there is a relative phase generated between these components once it interacts with the
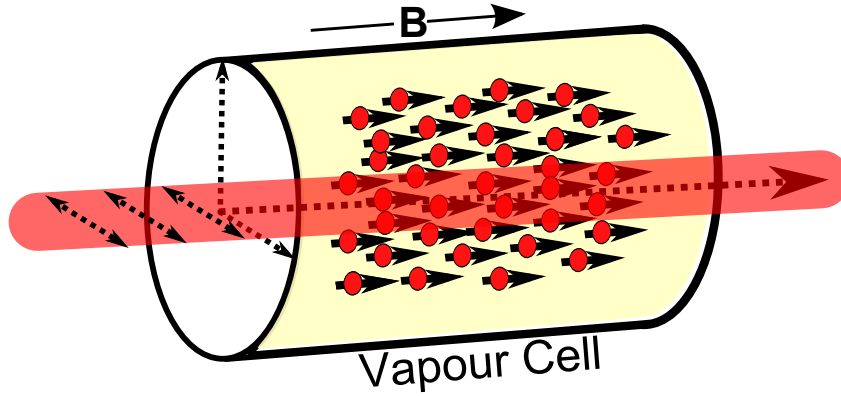
Figure 2.2: Linearly polarized light passing through atoms aligned towards z-axis

ensemble which will ultimately change the polarization of light. The amount of change in polarization is dependent on the degree of alignment of atoms. This effect is exploited to read the state of atomic ensemble. The amount of the rotation in the polarization of light transmitted will inturn tell the degree of alignment of atoms in the vapour cell.

2.4 State Preparation - Optical Pumping

As we saw in previous sections for performing quantum information tasks we first need a spin polarized ensemble of atoms. This is done be transferring the atomic population into $F = m_F$ hyperfine state which in case of ^{87}Rb is $5P_{1/2}, F = 2, m_F = 2$ state through a technique called as "Optical Pumping" which was first developed by the A. Kastler [15].

To understand the concept of optical pumping let us consider an atom with ground state $|g\rangle$ with $F = 1$ and excited state $|e\rangle$ with $F' = 1$. In presence of a weak magnetic field the hyperfine levels further get split up into $2F + 1$ sub-levels. When a resonant light is irradiated over the atoms the transitions are restricted by the selection rules (electric-dipolar transitions) given by

$$
\begin{aligned}
\Delta F &= 0, \pm 1 \\
\Delta m_F &= 0 \text{ for linearly polarized light} \\
&= +1 \text{ for } \sigma^+ \text{ polarized light} \\
&= -1 \text{ for } \sigma^- \text{ polarized light}
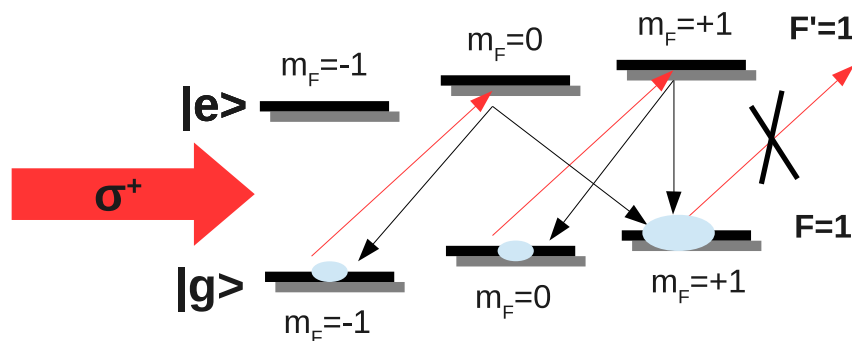\end{aligned}
$$

Figure 2.3: Optical pumping

16

If the resonant σ_+ light is irradiated over the ensemble of atoms in a weak magnetic field only the transitions with $\Delta m_F = +1$ are excited. This is considering that the Zeeman splitting which is proportional to applied magnetic field is considerably less than the line width of the incident laser otherwise the light will no longer remain resonant. The excited atoms then spontanously decay to the ground state in all possible ways $\Delta m_F = 0, \pm 1$ with decay probabilities proportional to Clebch-Gordan coefficients. In case of $5S_{1/2} \rightarrow 5P_{3/2}$ the life time in the excited state is 27.02 ns. So until the light is irradiated the atoms continuously excite and de-excite following the transition rules. Now consider an atom in the ground state with $F = 1, m_F = +1$, since only transition allowed is $\Delta m_F = +1$ and there is no $m_F = +2$ state in excited state the atom will not absorb the incident photon. So if an atom reaches the state $m_F = 1$ state it remains opaque for the incident light. Although atoms in other m_F states continue to absorb the light and some may eventually end up reaching the $m_F = 1$ state as shown in Fig. 2.3. This follows that over many cycles all the atoms get accumulated into the state of $m_F = 1$. Once all the atoms go to $m_F = 1$ no more light is absorbed by the ensemble of atoms. Thus most of the atoms get aligned in the direction of the magnetic field. This state is called a "dark state" of atoms since they are not going to absorb the incident light anymore and most of which is transmitted.

Although the atoms after getting pumped into the $m_F = 1$ state would not change their state by absorbing light, they can get relaxed into other Zeeman sublevels through various mechanisms like random collisions with walls, unpolarized atoms etc., So the statement that atoms get trapped in $m_F = 1$ state is only considering the electric-dipolar transitions. The amount of such relaxation of the spin of ensemble of atoms is characterized by the "Spin Relaxation Lifetime".

2.4.1 Spin Relaxation Lifetime

We saw in sec. 1.1.3 that storage time is one of the important metrics for the characterization of a quantum memory. In our system the storage time is characterized by the time for which the ensemble of atoms stays in a $F = m_F$ spin polarized state prepared by optical pumping. This is characterized as the decay of the total spin J_z, which follows the equation

$$J_z(t) = J_z(0)e^{-t/\tau} \tag{2.28}$$

where τ characterizes the lifetime of the collective macroscopic spin state of the vapour cell. A method to measure this lifetime is described in the experimental part of the next chapter. The relaxation of the spin lifetime takes place through various mechanisms which are briefly summarized in following section.

2.4.2 Relaxation Mechanisms

To achieve the desired metrics for a quantum memory described in sec. 1.1.3 an atom should be able to retain its spin state for a long time, losing which leads to the decoherence in the system. Few dominant mechanisms through which atoms lose their spin state are as follows

- **Collisions with walls** - This is the main mechanism where the atoms lose their spin. As the atoms are at the room temperature the rms velocity is of the order of hundreds of m/s which limits to the average time for an atom to stay before it

collides with the wall to be of the order of microseconds. So if the atom relaxes to other spin states every time when it collides with the wall the spin life-time is going to be in the order of microseconds. To overcome this the inner walls are coated with a type of paraffin - Tetracontane ($C_{40}H_{82}$). Rubidium atoms have elastic collisions with these coated walls and their spin lifetimes are increased. More details about this is discussed in the section on fabrication vapour cells in next chapter.

- **Collisions among the aligned atoms** - Since the atoms have non zeros spin, when they collide with each other there might be inelastic collisions resulting in exchange of spin. This can be reduced by introducing a buffer inert gas in the system, which have zero total angular momentum and collisions with these atoms do not change the spin state. Thus effectively increasing the mean free path of the atoms.

- **Reservoir effect** - Aligned atoms get exchanged with the atoms with arbitrary polarization from the Rb reservoir during the course of the experiment thus creating the decoherence. This can be reduced by decreasing the aperture size of the joint between the stem containing Rb reservoir and the main cell.

- **Collisions with other isotopes** - Rb has two isotopes ^{85}Rb and ^{87}Rb in the natural occurring mixture in the ratios of 3:1. So aligning one species will make the other unaligned and collisions with such atoms will lead to loss in spin. This effect can be reduced by the usage of isotopically enriched ^{87}Rb.

Other factors like the pressure, temperature inside the cell also play an important role in deciding the lifetime of the atoms.

Chapter 3

Experimental Details

In this chapter we are going to discusses in detail about the fabrication of tetracontane coated vapour cells, the laser systems and optical setup required for the characterization of spin relaxation. Later in this chapter a method to measure the spin relaxation life time is also described.

3.1 Fabrication of the Vapour cells

The fabrication of vapour cells has been investigated and the many techniques were developed over the past 50 years which were widely used in the field of atomic physics. As these vapour cells are used at room temperatures they showed high degree of decoherence. Many techniques were proposed to overcome this problem and get more spin relaxation time. One of the method proposed was to coat the cell walls with a paraffin derivative suggested initially by Norman Ramsay [16]. Different types of coating material were investigated over a number of years [17] It was found that coating the cell walls with long alkanes gave better results. Here we describe the procedure we used to prepare the vapour cells which similar to that as descried in [18]. Here we use tetracontane ($C_{40}H_{82}$) which is a paraffin derivative and commercially available.
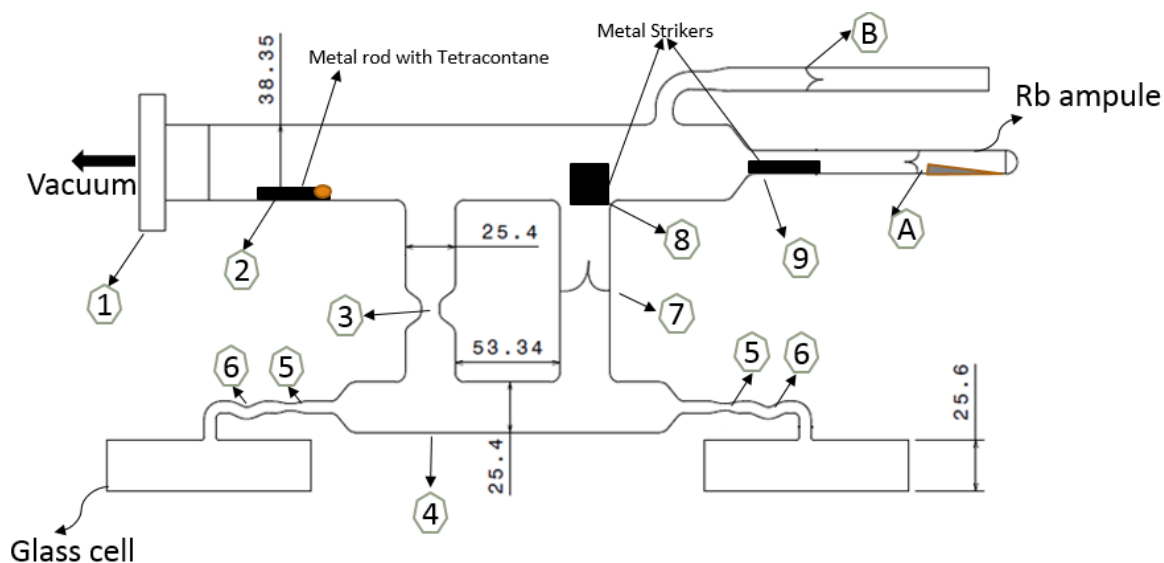

Figure 3.1: Design of the glass manifold made to prepare the Vapour cells

3.1.1 Glass Manifold

For the fabrication of vapour cells a glass manifold was designed and made of good quality pyrex (Corning 7740) whose schematic is shown in Fig. 3.1. This manifold consists of two glass cells which are cylindrical in shape, these are made by fusing 2 optical quality glass windows to a cylindrical tube. These glass windows are procured from Applied Optics Inc., Bengaluru[19]. These glass windows should be carefully fused to the cylindrical glass tube without any deformations which might change its curvature, upon which it would act like a lens destroying the collimation of incident light. A glass to metal flange whose glass end is made of pyrex is fused at (1) which is used to connect the manifold to the vacuum system. A Rubidium ampule procured from Alfa Aeser[20] is fused at (A) contains a 1 g of Natural mixture Rubidium ingot. Since Rubidium is highly reactive with oxygen and moisture, special care has taken in handling this ampule. The ampule is of total length 12.5 cm, 1 cm inner diameter and is made of borosilicate glass. It has a breakable seal which isolates rubidium from the atmosphere. There is another breakable seal at (7) which is broken using strikers placed at (8) and (9) during the course of the experiment. The constrictions at (5), (3) are to facilitate the pinching of glass.

3.1.2 The Vacuum System

Most important requirement while making these vapour cell is having a high vacuum inside the manifold. For evacuating the manifold to high vacuum of the order of 1×10^{-7} Torr both turbo molecular and scroll pump are used in conjunction. The scroll pump reduces the pressure to the order of 1×10^{-2} Torr upon which the turbo molecular pump is started to further evacuate the manifold. A Vacuum bellow and a value is used between the manifold and the vacuum system to facilitate easy manipulations of the manifold during the experiment.

3.2 Procedure

Now that we are ready with the main apparatus the procedure to make the vapour cells is described in this section.

Cleaning

Once the manifold is designed, before preparing the vapour cell, thorough washing of the manifold is necessary since many impurities and moisture get accumulated inside the manifold during the glass blowing. The manifold is washed using Distilled water, Dil. HCl, acetone, toluene, ethanol in sequence. It is then dried by heating with a hot blower under low vacuum achieved using a rotary pump via glass to metal flange at (1). It should be taken care that no moisture is left inside the manifold which would lead to degradation of vacuum.

Once dried, the manifold is detached from the system and a metal strikers which are fused inside glass tubes are carefully placed at (8) and (9). These are used to break the breakable seals at (7) and (A). Now small amount (around 10 mg) of tetracontane is deposited on an another such metal rod fused inside a glass. Two of such rods are used to take more amount of the coating material. To restrict the motion for these metal

rods a small magnet is fixed near every rod from outside the glass using a kapton (Heat resistant) tape.

Baking

The manifold is then connected to the vacuum system via glass to metal flange (1) and then pumped out to high vacuum of the order of 1×10^{-7} torr via the vacuum bellow. Manifold should thoroughly be checked for leaks (using leak detection) during the process of pumping out and the leaks should be properly closed either by glass blowing or using low vacuum sealant like Torr seal. To accelerate the process of pumping the manifold is to be properly baked which helps in degassing of any adsorbed impurities and reducing the base pressure. To bake the manifold it is wrapped with a layer of aluminium foil followed by wrapping with the heating tape and another layer of aluminium foil for uniform heating. The wrapping should be exempted at places where ampule at (A) and tetracontane coated rod placed at (2). Then the manifold is heated up to $150^{o}C - 200^{o}C$ using a heating tape. Two temperature sensors are kept at (4) and (9) to continuously monitor the temperature. The heating should only be started after the vacuum reaches its saturation and should be gradually increased at steps of $10 - 15^{o}C$. The manifold is kept at this temperature for 2-3 days under continuous vacuum pumping until it reaches the lowest possible base pressure. After this, the manifold is cooled to the room temperature gradually and then heating tape is removed.

Coating

Now we are ready to start the coating procedure. The metal rods at (2) is moved to the position (4) via (3) and then slight heat at (4) using hot air blower to melt the tetracontane onto the glass manifold. Once the material is transferred and then rod is cooled, it is taken back to (2) and the glass is pinched off (3) by heating carefully using oxy-fuel flame. Care should be taken at this point because the manifold can get punctured during the pinching in which case the procedure has to be repeated from start. At this point the part of the manifold below (3) and (7) is isolated from the other part. This is required so that the tetracontane doesn't escape while coating. Now this isolated part is again gradually heated up to $100^{o}C$ by wrapping the aluminium foil and heating tape. The heating should be considerably uniform so that coating would be uniform. Care should be taken that the heat gradient between the cells and other part should not be more than $5^{o}C$. Heating should be continued for few hrs until the deposited tetracontane gets completely vaporized and the vapours are uniformly spread along this isolated part of the manifold. Then it should be gradually cooled to room temperature and unwrapped. The coating is usually not visible to naked eye although visible white spots indicate the non-uniform coating in which case the procedure of heating should be repeated. The only way to check whether a coating is good or not is by placing a drop of water which will slide over the walls without sticking (though this cannot be done during this procedure).

After coating, the breakable seal at (7) is broken using the striker kept at (8) thus uniting the both isolated parts of the manifold. The coating material reacts with rubidium at high temperature so that Tetracontane should not be present in the path of the Rubidium. We need to remove the extra coated material from the manifold other than that of the cells. For this, the manifold is strategically heated so that the tetracontane

does not get deposit near the ampule. The manifold is wrapped in the regions (4)-(8)-(9), (5)-(4)-(5) leaving the other regions. Then it is gradually heated so that the extra tetracontane gets deposited towards (2) region. Care should be taken that it doesn't get deposited near (A) because heating in that region is not possible and after break opening the ampule entire rubidium will react with the tetracontane.

Depositing Rubidium and Pinching off cells

Once the tetracontane is removed from the path of the rubidium, the breakable seal at (A) is broken using the rod (driven using a magnet from outside) at (9). Then a small amount of Rb is carefully distilled from (A) to (6) over several steps. This acts as reservoir of Rubidium for the cell. Then the cells are pinched off from the manifold at points (5) using the oxy-fuel flame, after which the tips should be carefully annealed. Now we have 2 vapour cells successfully coated with the tetracontane. The tip containing the Rubidium should always be kept at lower temperature compared to the vapour cell body itself to avoid from Rubidium coating on the cell. As noted in [17] an additional "ripening" phase is required after the preparation of vapour cells where the cells are kept at $50 - 60^{o}C$ for few hours before the cell can exhibit for long relaxation times.

Disposing the Rubidium

After the cells are pinched off, the left over rubidium is then carefully transferred using distillation to the empty ampule (B). Then the ampule (B) is pinched off the manifold which can then reused as the ampule for further experiments. If it is not possible to transfer entire Rubidium into the ampule then the glass manifold should be carefully disposed. Opening manifold directly into the atmosphere might lead to uncontrollable exothermic reaction. To quench the reactivity of manifold it is filled with inert gas like Argon with positive pressure compared to atmosphere. Then manifold is disconnected with the bellow and quickly replaced with a blank flange. After this the manifold is kept in a box filled of dry ice and moved to some open place far from the experiment. Now carefully the flange is opened and atmosphere is allowed to react with Rubidium. After a while slowly water is filled into the manifold using a hose from a distance. After the fumes of the dry ice stop, the manifold can be recovered and cleaned properly to remove any traces of rubidium salts. Now the manifold can be reused for further experiments.

3.3   Measurement system

As we saw in previous chapter lifetime is one of the important characteristics for a vapour cell. These measurements require precise control over the lasers beams' stability, timings and control over magnetic fields. In this section we will be discussing various apparatus and equipment used for measuring the lifetime.

Laser

oscilloscope

AOM Controller

Solenoid

Coated Vapour Cell

Thorlabs
PD100A

oscilloscope

Optical Elements

Waveplate

PBS   λ/4 λ/2   Mirror   BS   AOM   Iris

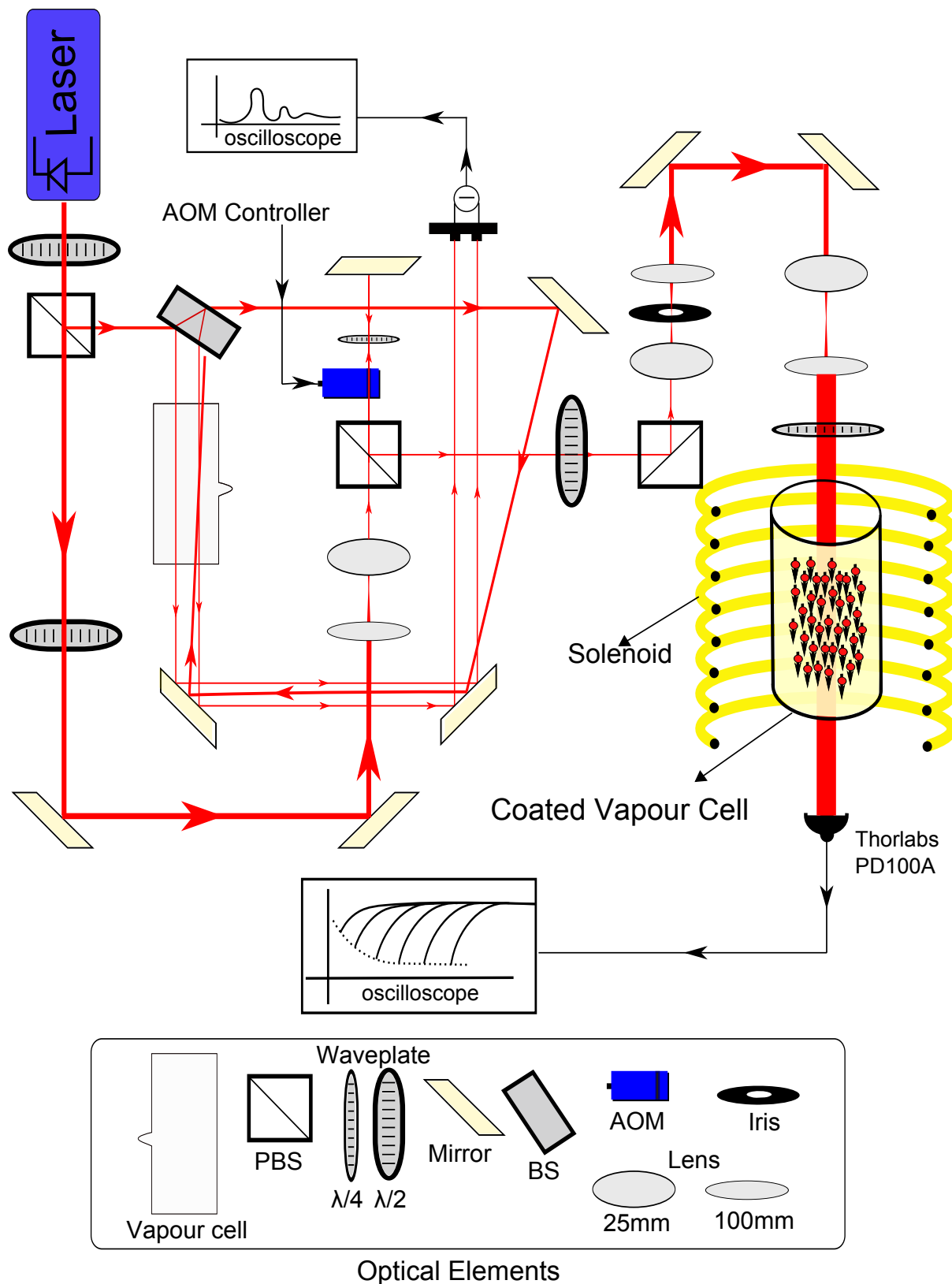Vapour cell   Lens   25mm   100mm

Figure 3.2: Schematic of Optical Setup

3.3.1 Laser

For the experiment a laser which is stable, tunable and has sufficiently narrow line width is required to be able to lock to one of the transition of Rb. In our experiments "Toptica DL Pro" laser is used with diode emitting light at wavelength "780nm". The construction inside the laser usually has a diode coupled with an angled grating whose position is controlled by a piezo. By applying DC voltage to this, one can be tune the frequency of the output. The laser is tunable up to few 10's of GHz by tuning the parameters like current, temperature, offset which are quite sensitive and should be carefully adjusted. For the experiments the laser needs to be locked to one of the transitions of Rb, without which the frequency might drift due to fluctuations in temperature and current. To do this a reference signal is required which is produced using a simple Rb vapour cell by a technique called saturation absorption spectroscopy.
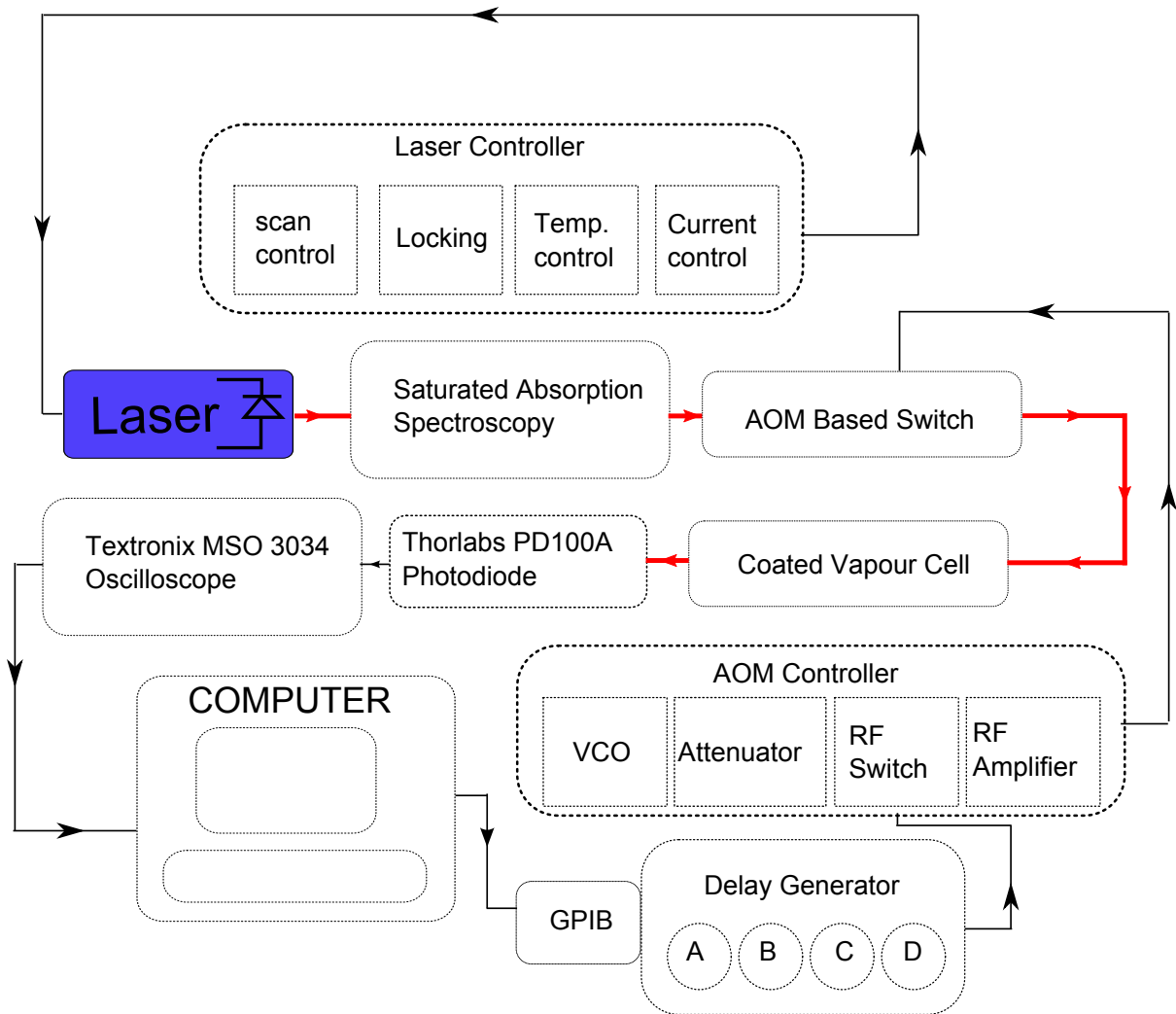

Figure 3.3: Layout of the experiment

3.3.2 Saturated Absorption Spectroscopy (SATABS)

Consider a laser light of 780nm is passed through a vapour cell and the transmitted light is recorded using a photodiode. If we scan the frequency of the laser and record

the spectrum over the scan, transmission profile shows the absorption peaks of various transitions of Rb. But as we are using the vapour cell at room temperature the velocity distribution of these atoms is given be the Maxwell Boltzmann distribution. An atom moving towards/away from the light sees a different frequencies. Thus such atoms might absorb the off resonant light such that the detuning compensates the Doppler Effect. This leads to the Doppler broadening of the transmission profile which is the convolution of transition and the velocity distributions. In room temperature the broadening is around 100's of MHz which engulfs many hyperfine transitions. To overcome we use saturation absorption spectroscopy which is a standard technique for removing the first order Doppler broadening.
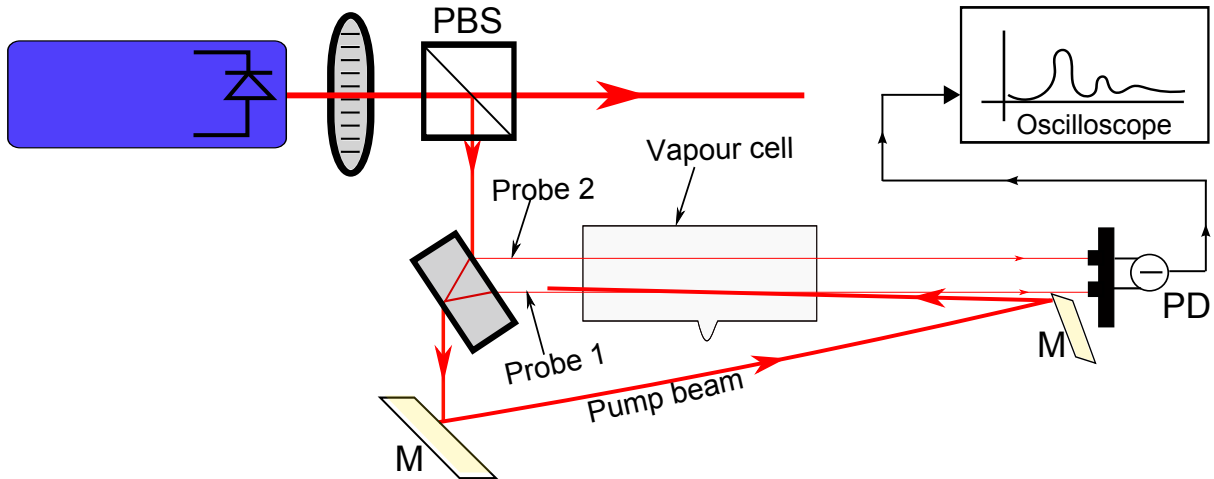

Figure 3.4: Saturated Absorption Spectroscopy

As we can see the schematic in Fig. 3.4. There are three beams which cross the vapour cell. The two weak beams (call *probe*1 and *probe*2) which are reflected from the thick glass beam splitter are recorded separately using two photo diode and their difference signal is shown in the oscilloscope. Another strong beam which overlaps the *probe*1 signal along the cell acts as a pump beam. Since these beams are counter propagating an atom moving with a velocity v either sees *probe*1 or *pump* beam as transition frequency but not both. But atoms with zero velocity sees both pump and probe beam at transition, since the pump beam is powerful it saturates the transition and reduces the absorption of *probe*1 beam creating a dip in its absorption. Thus if we subtract *probe*1 from *probe*2 we get the absorption peaks of zero velocity atoms. In addition few other peaks called cross over resonance peaks are also seen in the spectrum. This happens when two different transitions have frequency difference less than the Doppler broadening.

3.3.3 Laser Locking

Once we got the reference signal from SATABS, we need to lock the laser to the desired peak. The frequency stability of the laser is limited by the temperature stability of the environment, which leads to drifting of the laser frequency away from the desired one. So there should be a feedback given to the laser to correct this. To do this an error signal is generated by lockin amplifier whose modulation signal is fed to the laser. The frequency and amplitude of the modulation and gain should be played with to get an error signal with correct phase and amplitude. This error signal is then fed to a PID

controller, setting whose P, I, D values and gain, a DC signal is generated which is fed to the piezo of the laser. This signal corrects the frequency whenever it drifts from the peak. To lock to the desired peak it should brought to the center of the scanning range using the "Offset" and then scanning should be slowly reduced to zero followed by turning on the "PID" controller.

3.3.4 AOM based switch

For measuring the lifetime (described in next section) requires the ability to fast switching on/off of laser with switching times ranging from 100 μs to 1 ms with the resolution of 10μ s. This cannot be achieved using a normal mechanical shutter whose switching times would of range $500\mu s$. To achieve this an AOM(Acousto Optic Modulator) based switch is constructed. This scheme is motivated from the one described here [21]. An AOM works on the principle of Acousto-Optic effect and shifts the frequency of light using the sound waves. If RF electrical signal of frequency Δf and a laser of frequency f_0 is fed into the AOM the incident light frequency f_0 is shifted to $f_{\pm 1} = f \pm \Delta f$ based on the incident angle. At one incident angle either the frequency is shifted up or down i.e, only one of f_{+1} or f_{-1} are generated as shown in The shifted beam is slightly deflected
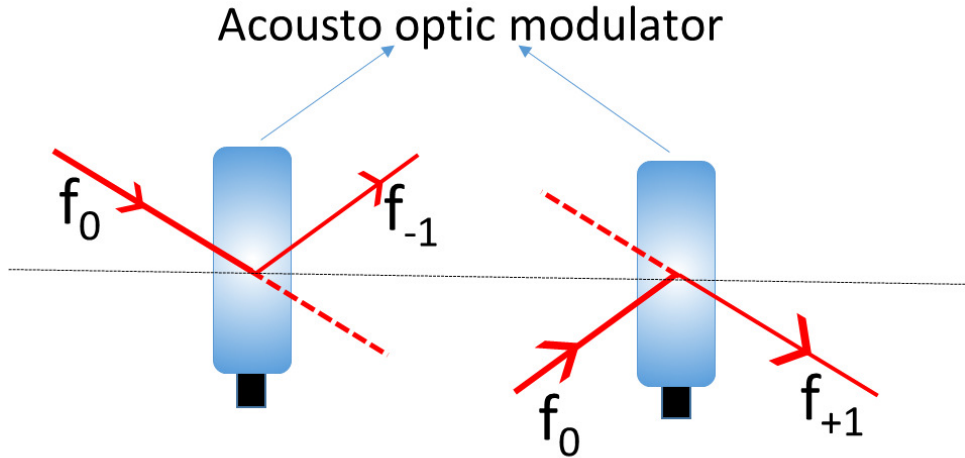

Figure 3.5: Usage of Acousto optic modulator

from the main beam whose deflection angle depends on the both f_0 and Δf. So by switching the RF signal on and off and blocking the f_0 light the $f_\pm$ can be switched on and off. But the problem is that the light which gets on and off has the frequency shifted away from the locked transition frequency. To compensate suppose we get f_{-1} after a single pass from the AOM and f_0 is blocked. This f_{-1} beam is sent back to the AOM using a mirror such that the f_{-1} is shifted up to get $f_{-1} + \Delta f = f_0$. Thus we get the f_0 back but in opposite direction. A "$\lambda/4$" is also kept between the AOM and mirror which will shift the polarization by $\pi/2$ after two passes. Thus the input and output light have a phase difference of $\pi/2$ which can be separated using a beam splitter. In the experiment we have use Intraaction AOM ATM80A2 which has maximum efficiency for RF input at 80MHz which requires RF input power of about 1.6W. The efficiency of the first order beam is usually $75 - 80\%$ which limits the efficiency to $55 - 65\%$ after the double pass configuration. This AOM is driven using a driver circuit which is built using
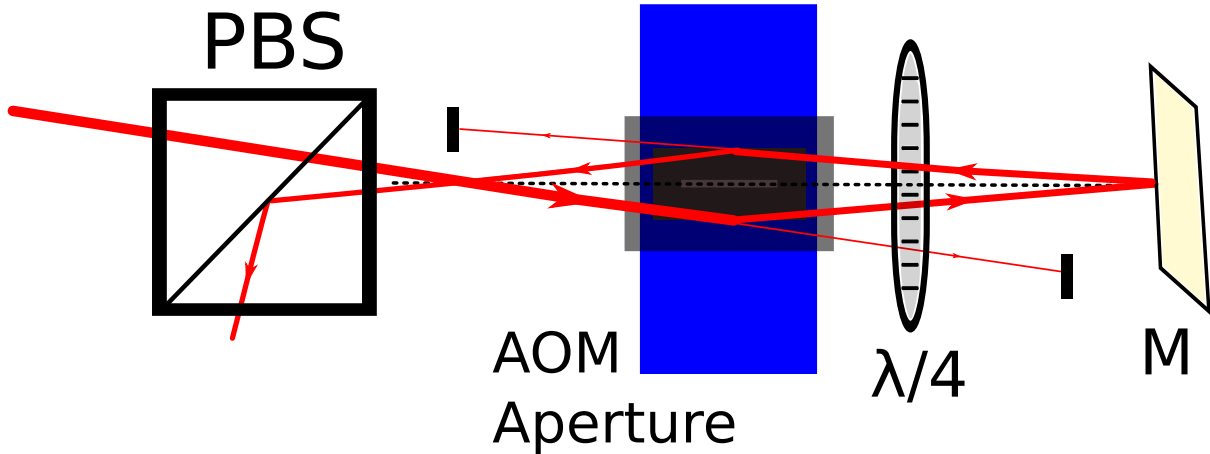
Figure 3.6: AOM based Switch

individual components from Minicircuits. The driver consists of a Voltage controlled oscillator (VCO) which can generate RF frequencies from $50 - 100$ MHz, then it has a Attenuator used to attenuate the signal amplitude, after that is a RF switch to turn the RF signal on/off and then followed by a 2W RF amplifier which amplifies the RF signal generated by the VCO. Both attenuator and the RF switch are controlled by an input analog signal from 0-17 V.

3.3.5 Delay generator

We have setup an AOM based switch which can be controlled by switching the RF signal through the RF switch, now we need to generate desired pulses in TTL form which controls the RF switch. For the experiment we need to continuously generate 2 pulses with tunable width and tunable delay between them. To achieve this a delay generator "SRS DG535" is used. A delay generator generates a trigger after a delay with respect to the external/internal trigger T. This module provides four such channels A, B, C, D whose trigger delay can be set with respect to either T or with each other. Boolean operations are applied on the four channels A, B, C, D to get the desired output $O = (A-B)\vee(C-D)$ using simple logic gates. The complete usage of this given in detail in next chapter.

3.3.6 Magnetic fields

To generate the quantization axis for the vapour cell during the course of the experiment a magnetic field is created using a solenoid of length around 19cm and diameter 12cm. This can generate around 10 G/A of Magnetic field. Additionally 4 other coils are used in Helmholtz configuration to compensate the earth's magnetic field along the directions perpendicular to the axis of the cell.

3.3.7 Control, Automation and Acquisition

During the course of the experiment the transmitted light is recorded from the vapour cell using a Thorlabs PD 100A photodiode at suitable gain, and fed to the Tektronix MSO 3034. The data from the oscilloscope is acquired using a computer via an usb cable. The delays to the delay generator is set from the computer using a GPIB interface. LabVIEW

modules to control these devices and record the output of the photodiode is written. The front panel of the program is shown in the Fig. 3.7
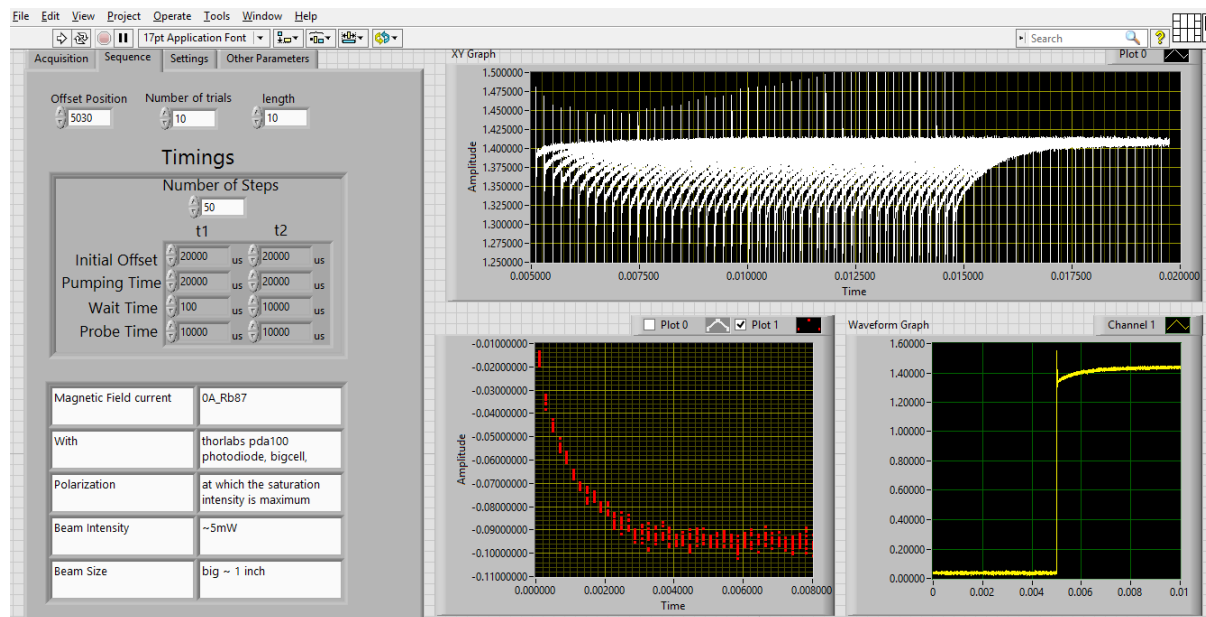

Figure 3.7: LabVIEW program to measure the Spin Relaxation time

3.4 Measuring the spin relaxation times - Relaxation in Dark

In this section we briefly describe a technique to measure the spin relaxation lifetime of ensemble of atoms in a vapour cell. If a σ^+ light at frequency of transition of atoms as mentioned in sec. 2.4 is irradiated, via optical pumping the atoms get populated into one of the Zeeman sublevels after which no more light is absorbed making the vapour transparent to the incident radiation (as shown in (a), (b) of Fig. 3.8). Now the lifetime can be measured by allowing the aligned atoms in the vapour cell to relax in absence of light ((c), Fig. 3.8). During the relaxation time, the atoms lose their alignment (spin) due to various reasons mentioned in 2.4.2.
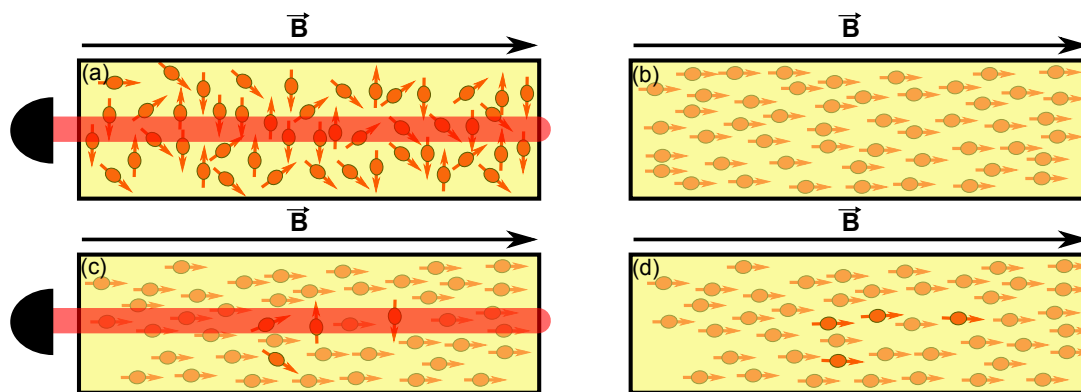

Figure 3.8: Franzen Sequence

The incident light is blocked using the AOM switch described in sec. 3.3.4 for a given time say t_i. After that the σ^+ polarized resonant light is again irradiated on the vapour cell. Because of the partial relaxation during this time the transparency of vapour decrease for a moment and then the atoms get pumped back restoring the transparency((d), Fig. 3.8). This can be seen by momentary dip in the voltage signal initially from the photodiode. Now if we record this signal I_i just after the switch is closed and take different sets of I_i by varying the delay time t_i we can see that the profile of I vs t follows an exponential decay pattern given by

$$I = I_0 e^{-t/\tau} \tag{3.1}$$

Thus we obtain the relaxation time τ of the vapour cell by fitting the above equation to the obtained result. This technique is called "Relaxation in Dark" first proposed by W. Franzen [16]. Detail description of this measurement is described in next chapter.

Chapter 4

Results

4.1 Fabrication the vapour cells

Using the method discussed in previous chapter 3.1, vapour cells shown in the Fig. 4.1 were fabricated. Initial attempts at coating the vapor cells with tetracontane (paraffin) were unsuccessful. However, Rb vapor was distilled successfully into the vapor cells. About six attempts of coating the vapor cells with paraffin were made. The failure of the paraffin coating was seen through the spin relaxation time measurements as outlined in the next section.

Figure 4.1: First pair of Rubidium vapour cells fabricated at IISER Pune

4.2 Measurement of spin relaxation lifetimes

In last chapter we discussed a technique used to measure the life time of a spin polarization of gas ensemble in a vapour cell. In this section we will show some results of such a measurement. Vapour cell is kept at room temperature under a constant bias magnetic

field generated by a solenoid of diameter 12cm and length 19cm . The solenoid is capable of generating around 10 G/A magnetic. The experiment is done with 3 different vapour cells with following configurations.

1. Coated vapour cell of length 5cm and diameter of 7cm referred as "Cell-A" in the discussion henceforth.

2. Uncoated coated vapour cell prepared in-house of length 10cm and diameter 2.5cm is referred as "Cell-B"

3. Uncoated commercial(Toptica Photonics) vapour cell having length of 5cm and diameter 2.5cm is referred as "Cell-C"

The spin relaxation time of optically pumped Rb atoms is measured by the following protocol. Initially atoms are optically pumped into the $F = 2, m_F = 2$ state of the ground $5S_{1/2}$ state. A circularly polarized laser light, whose frequency is locked to the $5S_{1/2}F = 2 \rightarrow 5P_{3/2}, F = 3$ transition is used for the optical pumping. The entire optical pumping and detection is performed as shown in the timing diagram below (see Fig. 4.2). Optical pumping is done during the period labeled "Pump Time". During this time, atomic spins are oriented along the quantizing magnetic field. After a certain time labeled "wait time Δt ", the probe field is turned on and intensity of the transmitted light is measured.

During the "wait time" the atomic spins will relax and will have a mixture of polarized and unpolarized components. The unpolarized component will increase with increase in "wait-time". When circularly polarized light is incident on the sample and goes through the cell, the intensity of the absorption of the light is proportional to the unpolarized component. For larger wait times, the strength of the transmitted light reduces, hence, becomes an indicator of the depolarized component. By varying "Δt" we get a profile of how the atoms get relaxed over time after optical pumping, which in turn gives the lifetime of spin relaxation. A sequence of measuring the life time is thus divided into such (pump, wait, probe) cycles that are controlled by the AOM switch.
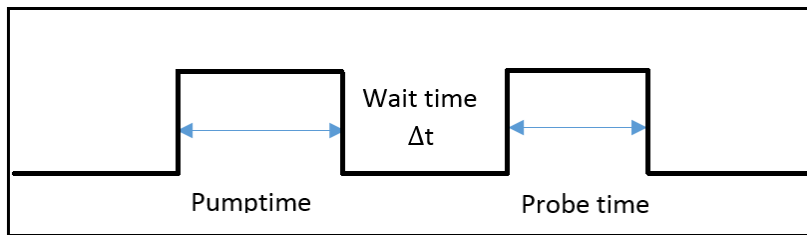

Figure 4.2: Switching sequence

To record the measurements, pump and probe pulses are generated by electronic switching of the RF given to the AOM based optical shutter. The electronic pulses are generated using a digital delay generator. The optical intensity is recorded through a data acquisition using Textronix MSO 3034 digital storage oscilloscope. The oscilloscope is triggered at the rising edge of the probe pulse and the intensity of the probe pulse is recorded by averaging the oscilloscope signal in $10\mu s$ time window. The graph below describes such a measurement done using the "Cell-A" under bias magnetic field of 1.5 Gauss. The width of pump and probe pulses are set at 20 ms and wait time is varied

from 100 μs to 10 ms. The exponentially increasing ramps showed in the graph are transmission of the probe pulse which are plotted by setting the falling edge of the pump beam as origin and varying the wait time. The intensity is recorded just after the rising edge of the probe beam and then subtracted from the saturation intensity.

Those differences for different wait times is recorded and then fitted to an exponential ramp of form $y = a * e^{(-t/\tau)} + b$ and then the $1/e$ life time (τ)is obtained. This lifetime curve is showed in red line in the graph below.
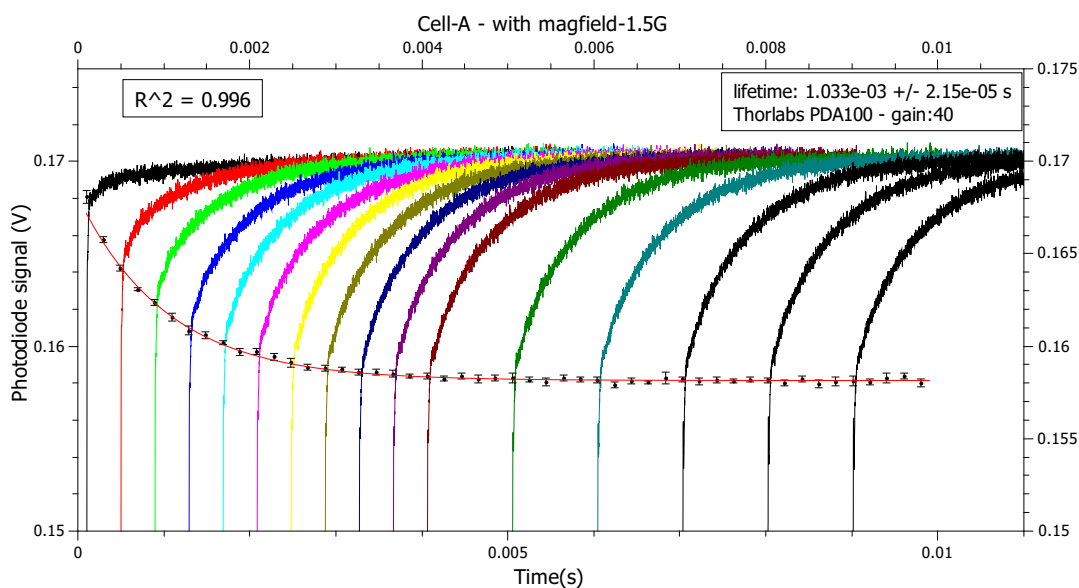

Figure 4.3: Measuring the lifetime of vapour cell: The ordinate shows the photodiode signal that is proportional to the transmitted light. The ordinate shows the time axis. Different coloured curves show the photodiode signal at different wait times.

The life time measurements were different at different magnetic fields as shown the following figure. As seen from the data, the fraction of optically pumped atoms does not get affected significantly by the increasing magnetic field. This is due to the fact that, optical pumping demands that Zeeman energy shift of the various magnetic sublevels should be within the natural line width. If the Zeeman energy level shift is greater than the natural linewidth, only a small fraction of the atoms would be in resonance with the laser light. For comparison the lifetime curve obtained from previously described method without any vapour cell is also plotted as "CellA-nocell". The curve "CellA-detuned" is lifetime curve when the input laser light is slightly detuned from the transition which also has similar lifetime but has low number of pumped atoms. Similar measurement was done with ^{85}Rb by locking the laser to $5S_{1/2}F = 3 \rightarrow 5P_{3/2}, F = 4$ transition, but no significant difference was observed in the spin relaxation time.
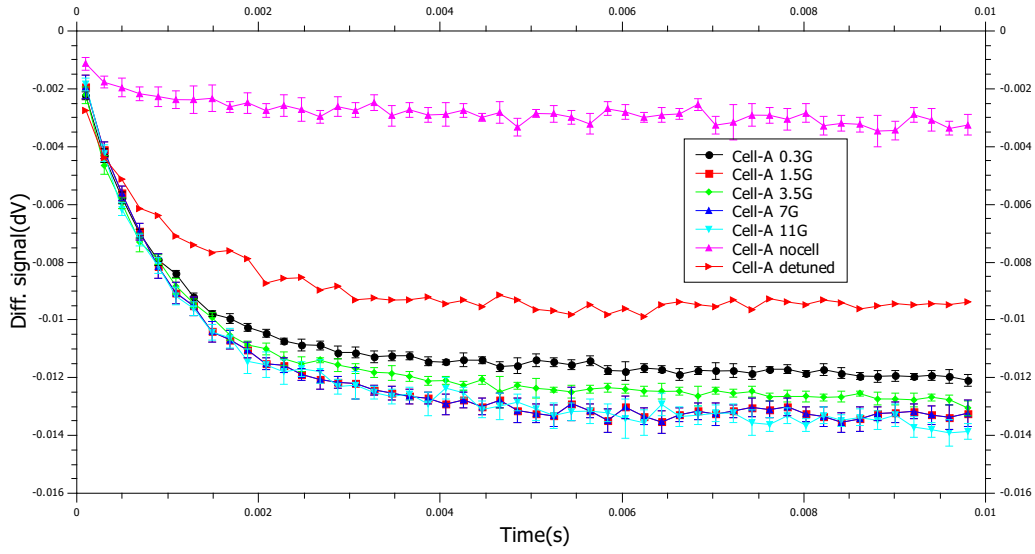
Figure 4.4: Lifetime at various bias magnetic fields

The pumping rate and population in desired state seems to vary with magnetic field, but there is no observed trend in the variation of lifetime w.r.t the applied magnetic field.

Table 4.1: Spin relaxation time vs Magnetic field

Coil Current	Mag Field	1/e Lifetime (ms)
0A	0.3G	0.944(2)
0.15A	1.5G	1.10(2)
0.3A	3.5G	1.08(3)
0.6A	7G	1.10(2)
1A	11G	1.08(4)

For comparison similar lifetime curves are plotted for Cell-A, Cell-B and Cell-C.
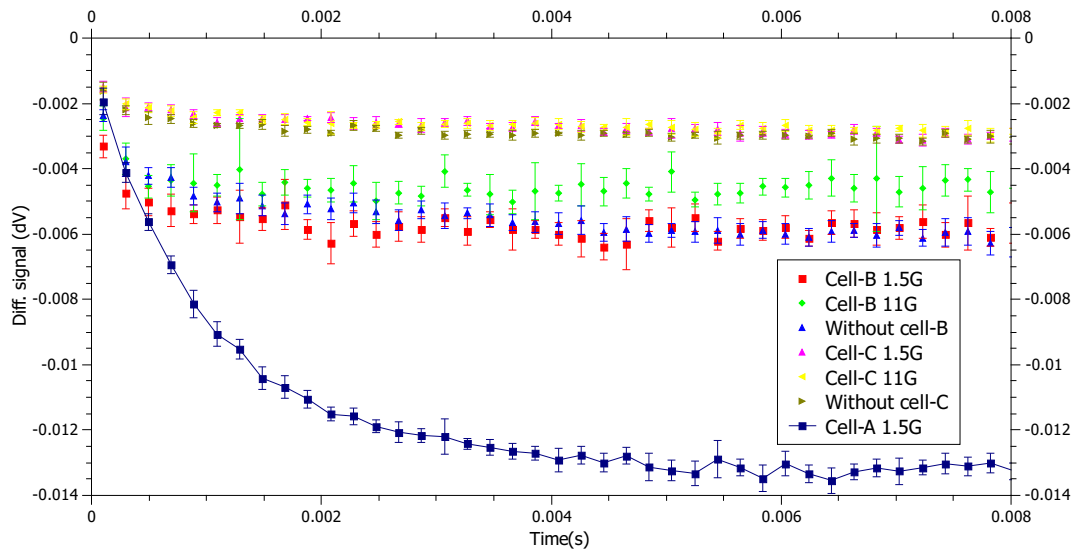

Figure 4.5: Comparision of lifetimes

Chapter 5

Discussion

As we saw in previous chapter the measured spin relaxation lifetime of the ensemble of atoms in vapour cell is around 1 ms. But many groups have reported lifetime of order of 100's of milliseconds. The reason for this may be due to poor quality of coating or usage of the natural rubidium mixture instead of isotopically enhanced rubidium. The fabrication of the vapour cell involves in handling of sensitive and fragile glass manifold whose breakage leads to repetition of entire tedious procedure again which spans for about 7-10 days. Few of the major problems we faced during the fabrication were

- During the process of glass blowing for preparing the manifold, some dust particles get trapped inside the glass creating micro-cracks which leads to leakages that are prominent at the vacuum level of 1×10^{-4} to 1×10^{-7} Torr. So, proper leak check of the manifold has to be done before starting the baking process.

- The annealing has to be done carefully at the joints, failure of doing which might result in the breakage of the manifold during the baking process or while distilling the Rb.

- An insulated heating tape was used for heating the manifold during baking and coating processes. The bulkiness of the tape doesn't allow us to uniformly heat the manifold at all places, which results in cold spots leading to the accumulation of tetracontane. To resolve this a better heating facility like building a dedicated oven with continuous air flow or a thinner heating tape has to be used which can maintain uniform temperature.

- Next problem was in distilling the Rb from the ampule to the reservoir of the cell. This was done by breaking the seal of the ampule, careful manipulation of the manifold and guiding the Rb vapour using a hot air blower. But due to the vacuum bellow connection the manipulations of the manifold were restricted. To solve this issue a flexible bellow connection has to be used or the design of the manifold has to be revised such that it can be detached from the vacuum during the coating, distilling processes and can be reattached just before pinching off the cell from the manifold without compromising the vacuum inside the manifold.

There were few other minor problems during the fabrication, the process of resolving them and improving the fabrication process is currently in progress.
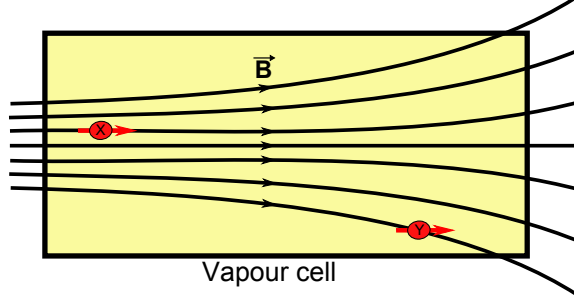
Figure 5.1: Vapour cell in a non-uniform Magnetic Field

Another reason which lead to the measurement of low spin relaxation time is the non-availability of uniform magnetic field across the cell. In the current experimental condition there was a fluctuation of magnetic field of order of 0.1 Gauss over a distance of 2 cm. Consider an atom getting pumped at one place (say "x" in Fig. [5.1]) with the magnetic field as quantization axis, after a while if it reaches a place(say "y" in Fig. [5.1]) where the magnetic field is oriented along a different direction then it will again try to align itself to that direction in presence of the circularly polarized light. So, after the wait time when we measure the transparency it may be the case that few aligned atoms didn't lose their spin due to random collisions but the reason might be that the magnetic field at the new location is different than the time when they were pumped. This way we might be under estimating the life time of the vapour inside the cell. To resolve this issue a multilayered mu-metal magnetic shield which can provide milliGauss level shielding from external stray magnetic field has to be used.

The measurements till now were made in the pure state ($m_F = +2$, $F = 2$) of the ^{87}Rb ensemble which was prepared using a resonant σ^+ polarized light. Similarly the atoms can be pumped to ($m_F = -2$, $F = 2$) using a resonant σ^- polarized light. To create a superposition of these two states a pair of lasers in the Raman configuration can be used to coherently couple the ($m_F = -2$, $F = 2$) and ($m_F = +2$, $F = 2$) Zeeman sublevels (as shown in Fig. [5.2]). The first laser is locked to the transition ($m_F = -2$, $F = 2$, $5S_{1/2}$) $\rightarrow$ ($F = 3$, $5P_{3/2}$) and the other to the transition ($m_F = +2$, $F = 2$, $5S_{1/2}$) $\rightarrow$ ($F = 3$, $5P_{3/2}$) both having a detuning Δ. This can also be achieved by using a RF wave whose energy is equal to the energy difference of the two Zeeman sublevels. Thus using such configuration the lifetime measurements can be done for any superposition of the Zeeman levels.
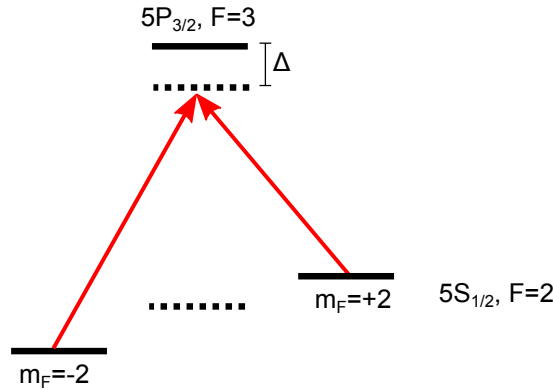

Figure 5.2: Pair of Raman lasers coupling the Zeeman sublevels of ^{87}Rb

Till now we have been measuring the longitudinal relaxation time on the ensemble of atoms (T1) which is the relaxation of the component J_z. This quantifies the lifetime of atoms if the are in the pure state of $m_F = +2$. But in a state of superposition the storage time also depends on the time till which the Zeeman levels are coherently coupled. This is quantified by the transverse coherence time (T2) which can be measured using the Double resonance Optical method or "Ramsey Measurement" [14]. The transverse lifetime (T2) is also affected by the relaxation mechanisms discussed in sec. 2.4.2 and it is known that typical T2 lifetime is much less when compared to the T1 lifetime, which would be in the order of microseconds in our case and cannot be effectively measured using the current setup. Once the T1 lifetime is optimized, efforts have to be made to optimize the T2 lifetime along with the other metrics discussed in sec. 1.1.3.

5.1   Future plans

With the current stage we have understood the problems in making vapour cells and established a protocol to fabricate them. We have an experimental setup to measure the spin relaxation life time with good accuracy. We would further like to improve these measurements by using a magnetic shield which would shield the vapour cell from external magnetic field fluctuations thus decreasing the decoherence. An improvement in the protocol of fabrication is also required to improve the coating qualities. We would also like to try other possibilities like using a buffer gas inside the cell which would also lead to better lifetimes. Once we fabricate a cell which exhibit the life time of the order of few 100's of milliseconds, we would then try to implement memory using the off resonant interaction scheme. The next goal would be to improve the other metrics of quantum memory and show basic phenomenon like entanglement, teleportation and build schemes to create the quantum gates and operations. There are many interesting physics phenomenon like Electromagnetic Induced Transparency which can be observed using these vapour cells. Thus we conclude that this field has many more exciting things to explore and only few of them have been achieved till now.

References

[1] N. D. Mermin, Quantum computer science, Cambridge University Press.

[2] S. Wiesner, Conjugate coding, SIGACT News 15(1) (1983) 78–88.

[3] B. Omer, Structured quantum programming, http://tph.tuwien.ac.at/~oemer/doc/structquprog.pdf.

[4] D. P. DiVincenzo, The physical implementation of quantum computation, arXiv:quant-ph/0002077.

[5] L.-M. Duan, M. D. Lukin, J. I. Cirac, P. Zoller, Long-distance quantum communication with atomic ensembles and linear optics., Nature 414 (2001) 413–418.

[6] B. Julsgaard, A. Kozhekin, E. Polzik, Experimental long-lived entanglement of two macroscopic objects., Nature 413 (2001) 400–403.

[7] C. Liu, Z. Dutton, C. H. Behroozi, L. V. Hau, Observation of coherent optical information storage in an atomic medium using halted light pulses., Nature 409(6819) (2001) 490–493.

[8] D. F. Phillips, A. Fleischhauer, A. Mair, R. L. Walsworth, M. Lukin., Storage of light in atomic vapor, Physical Review Letters 86(5) (2001) 783–786.

[9] A. I. Lvovsky, Optical quantum memory, Nature Photonics 3 (2009) 706–714.

[10] M. Fleischhauer, M. D. Lukin., Dark-state polaritons in electromagnetically induced transparency., Physical Review Letters 84(22) (2000) 5094–5097.

[11] R. Loudon, The Quantum Theory of Light, Oxford Science Publications, 2001, Ch. Quantization of the radiation field, pp. 125–144.

[12] D. A. Steck, Rubidium 87 d line data, /http://george.ph.utexas.edu/~dsteck/alkalidata/rubidium87numbers.pdf.

[13] D. A. Steck, Rubidium 85 d line data, /http://george.ph.utexas.edu/~dsteck/alkalidata/rubidium85numbers.pdf.

[14] B. Julsgaard, Entanglement and quantum interactions with macroscopic gas samples, http://phys.au.dk/fileadmin/site_files/publikationer/phd/Brian_Julsgaard.pdf.

[15] W. Happer, Optical pumping, Reviews of Modern Physics 44 (1972) 169.

[16] H. G. Robinson, E. S. Ensberg, H. G. Dehmelt, Investigation of antirelaxation coatings for alkali-metal vapor cells using surface science techniques, Bull. Am. Phys. Soc. 3 (1958) 9.

[17] S. J. Seltzer, et. al., Investigation of antirelaxation coatings for alkali-metal vapor cells using surface science techniques, The Journal of Chemical Physics 133 (2010) 144703.

[18] G. Singh, P. Dilavore, C. O. Alley, A technique for preparing wall coated cesium vapor cells, Review of Scientific Instruments 43 (1972) 1388.

[19] Bengaluru, Applied optics, http://www.appliedoptics.net/.

[20] Rubidium, Alfa aesar, https://www.alfa.com/en/docs/prod_instruct/10315.pdf.

[21] W. J. Schwenger, J. M. Higbie, High-speed acousto-optic shutter with no optical frequency shift, REVIEW OF SCIENTIFIC INSTRUMENTS 83 (2012) 083110.